Improving techniques for Shack-Hartmann wavefront sensing: dynamic-range and frame rate

Takao Endo, Yoshichika Miwa, Jiro Suzuki and Toshiyuki Ando
Information Technology R&D Center, Mitsubishi Electric Corporation
5-1-1 Ofuna, Kamakura, Kanagawa 247-8501, Japan

Takashi Takanezawa and Yutaka Ezaki
Communication Systems Center, Mitsubishi Electric Corporation
8-1-1 Tsukaguchi-Honmach, Amagasaki, Hyogo 661-8661, Japan

ABSTRACT

A Shack-Hartmann wavefront sensor (SHWFS) is one of the most popular sensor for testing large telescope optics, real-time wavefront measurement, and atmospheric turbulence compensation used in adaptive optics. In adaptive optics, wavefront sensing often requires to deal with large wavefront aberration disturbed by atmospheric turbulence. However, the dynamic-range and frame rate of conventional SHWFS are restricted by the size of lenslets and amounts of readout pixels, respectively. In this paper, we propose two main approaches, (1) switching the user defined region of interest (ROI) to achieve over kHz frame rates, and (2) spots pairing algorithm to increase the dynamic-range of SHWFS.

First of all, an array of focused spots of each lenslets, which is called Hartmanngram, is also distorted when incident wavefront has large aberration. Therefore, we implement a simple algorithm to determine the relation between the lenslets and the focal spots. To confirm the algorithm, the testing lenses are designed, as it is capable to generate an appropriate defocus and spherical aberration. Using the proposed algorithm, a distorted wavefront, such as defocus aberration of 11 μm and spherical aberration of 7 μm, can be successfully measured. Furthermore, in order to verify the linearity and dynamic-range of proposed SHWFS, the coma aberration which increases in proportion to the decentering of the testing lenses is also measured. In conclusion, the residual wavefront error of 0.2 μm is estimated in the range of coma aberration of $\pm$10 μm.

In order to improve frame rate, we next define two typical ROI region for normal and crop readout mode reducing the number of readout pixels. Each readout mode can be quickly switched within 10 ms in proportion to slope of incoming wavefront. As a result, the frame rate in crop mode is improved twice faster from 2 kHz to 4 kHz, and the repeatability of wavefront error is satisfied < 6 nm RMS.

1. INTRODUCTION

A Shack-Hartmann wavefront sensor (SHWFS) is one of the most common methods used to characterize the wavefront aberrations of an optical system [1]. It is also widely used for wavefront sensing in astronomical adaptive optics imaging (AOI) system. For example, SHWFS can be used for optical testing of space/ground based telescope [2; 3], measuring laser beam quality, and human eye aberrometer for LASIK surgery.

In these optical testings, the wavefront can be generally measured and reconstructed in the order of a few seconds to a few minutes. However, wavefront sensing in an AOI system is used for real-time operation. As it is discussed later, the frame rate of SHWFS is limited by the readout speed of two dimensional imaging device. On the other hand, the dynamic range of SHWFS depends on the size of sub-aperture lens.

In this paper, in order to improve measurement performance of SHWFS, we introduce two main techniques: (1) method for expanding the dynamic range and (2) method for increasing the frame rate.

1.1. Principle of Shack-Hartmann wave sensing

At first, we explain the principle of measuring wavefront of SHWFS. The SHWFS is a pupil plane measurement of local wavefront slopes (the first derivative of the wavefront) within a sub-aperture defined typically by a lenslet array. The segmented incident wavefront focuses a spot onto an array of detectors such as CCD or CMOS image sensor in the lenslet focal plane. The positions of the focal spots (generally called Hartmann spots or Hartmanngram) on the position detector are proportional to local wavefront slope.

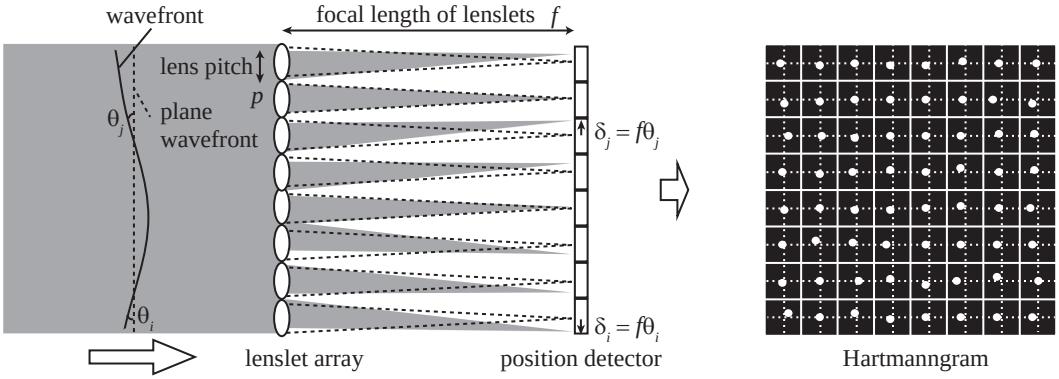

Fig. 1. Principle of Shack-Hartmann wavefront sensing technique

The right portion of Fig. 1 shows that the location of the spot focused on the detector, δ_i is related to the local wavefront tilt θ_i over the ith sub-aperture as follow.

$$\delta_i = f\theta_i \tag{1}$$

where f is the focal length of the sub-aperture lens. The spot location δ_i is estimated by calculating the centroid of the spot on the detector plane [4]. The performance of SHWFS depends on size of sub-aperture lens (pitch of lenslet p), distance from lenslet to focal plane, pixel size of position detector, and signal to noise ratio.

From the equation (1), the fundamental limitation is caused by a tradeoff between dynamic range and measurement sensitivity. For example, measurement sensitivity depends on the focal length of lenslet f, the dynamic range is limited by the pitch of lenslets p, because the displacement $|\delta| < p/2$ is required. This point will be described in the following section.

1.2. Hartmanngram and reconstructed wavefront

Next, Fig. 2(a)–(b) show examples of Hartmanngram and reconstructed wavefront for positive or negative defocus aberrations, respectively. The green square cells in Fig. 2 shows the lenslet used for a wavefront reconstruction. The positions of focal spots (white point) around the center of Fig. 2 are aligned at the center of green square cells. However, focal spots at the outer annulus of Hartmanngram are gradually shifted to inner/outer edge of sub-aperture. If the focal spot displace out of sub-aperture, multiple spots or crossed-over spots could appear within the same centroiding area. Therefore, the dynamic range for conventional SHWFS is limited by the condition of $|\delta| < p/2$.

In order to improve measurement performance of SHWFS, we thus introduce two main techniques: (1) method for expanding the dynamic range and (2) method for increasing the frame rate. First, the concept model of wide dynamic range SHWFS which can be measured up to 11 μm of defocus, 6.9 μm of spherical aberration, and 12.7 μm of coma aberration, as discussed in section 2. Next, we also discuss about 4 kHz frame rate SHWFS obtained with 10×10 Hartmanngram in section 3.

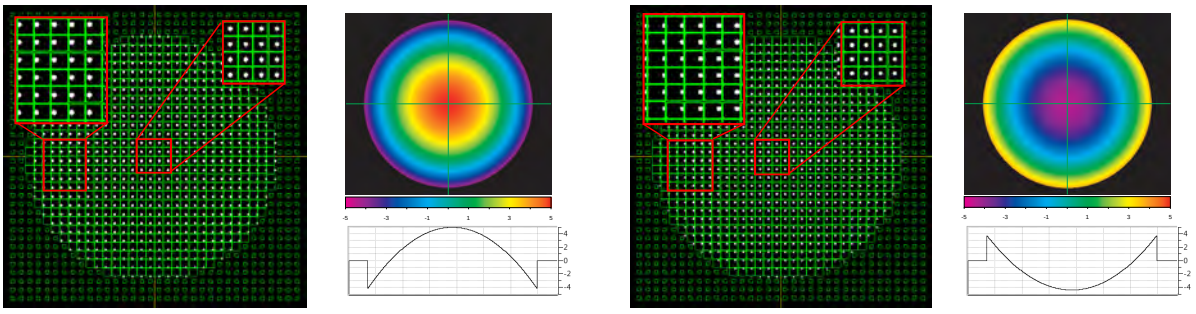

(a) (b)

Fig. 2. Example of Hartmanngram and reconstructed wavefront – positive and negative defocus.

2. Techniques for expansion of dynamic range

In order to expand dynamic range, we first have to resolve the following two problems: (1-a) the non-uniform illuminance distribution of Hartmanngram, and (1-b) the connection algorithm between Hartmann spots and related sub-apertures.

The former problem is derived from the steepness of incoming wavefront slope because the illuminance on position detector decrease with increasing the incident angle of θ_i. Fig. 3(a) is an example of Hartmanngram of highly distorted wavefront. In Fig. 3(a), white points indicate focal spots. The illuminance of focal spots around the center of Hartmanngram are saturated. On the other hand, the illuminance of focal spots at outer annulus are relatively faint, so the SNR of these spots is not enough accurate for centroid calculation.

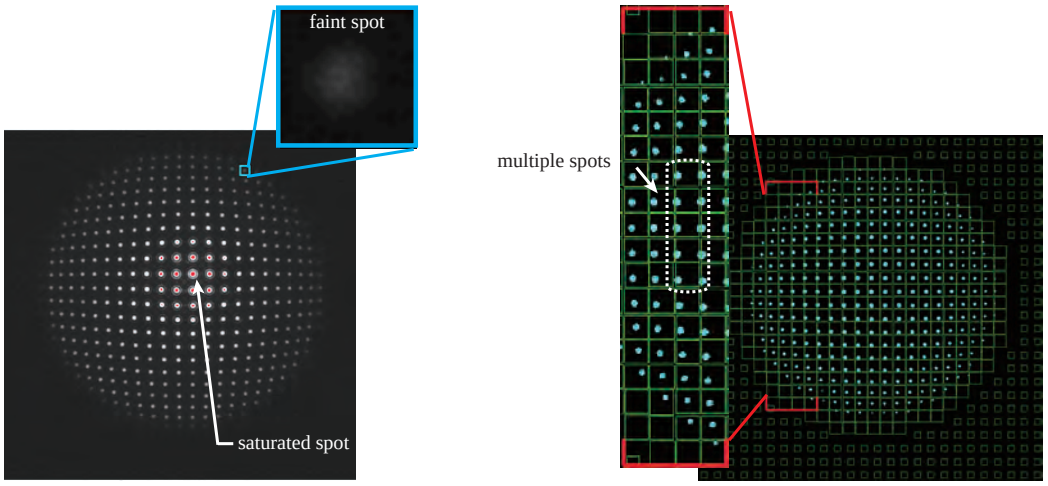

(a) (b)

Fig. 3. Example of Hartmanngram – (a) non-uniform illuminance distribution, (b) multiple spots.

The accuracy of the wavefront slope δ depends on the accuracy of the centroid calculation of focal spot. However, both the saturated spots and the faint spots cause some difficulties in the determination of center of gravity. Therefore, illuminance distribution of Hartmanngram should be uniform. We will discuss the techniques of improvement of illuminance in section 2.1.

Next, the displacement of the focal spot δ_i is proportional to incident wavefront slope θ_i. If the incident wavefront is

plane wave, the position of focal spots is the center of lenslet. However, increasing the slope of wavefront θ_i, the focal spot displace out of the footprint of the ith sub-aperture. Fig. 3 shows the pattern of focal spots obtained from a highly distorted wavefront at the condition of spot displacement $|\delta| \geq p/2$. In Fig. 3, white points indicate focal spots and green squares also indicate the size of sub-aperture lens. In this case, multiple spots shown with the white dotted circle in Fig. 3 can be seen in the same sub-aperture. In order to avoid mismatch of these multiple spots, we will discuss the techniques of connection between Hartmann spots and the related lenslets in section 2.2.

Note that the design parameters of testing SHWFS used in section 2 are summarized in Tab. 1.

Tab. 1. Specifications of testing SHWFS.

Item	Specification
Number of sub-apertures	24×24
Upper spatial resolution	10 th order Zernike mode
Interval of lenslets	0.3 mm
Focal length of lenslets	20 mm
Image sensor type	CMOS image sensor
Frame rate	20 fps
Dynamic range	18 λ@1064 nm
Accuracy	< 5 nm RMS
Number of readout pixels	1056×1056

2.1. Improving SNR of non-uniform Hartmann spots

In order to improve uniformity of Hartmann spots, we propose a method of acquiring multiple frames with increasing/decreasing the time of exposure, and accumulating uniform spots from which both saturated and faint spots have been removed [5]. The method is also used for High Dynamic Range (HDR) imaging for digital camera etc. Left upper rows of Fig. 4 shows example of Hartmanngram obtained with increasing the time of exposure ($t_1 < \cdots < t_5$).

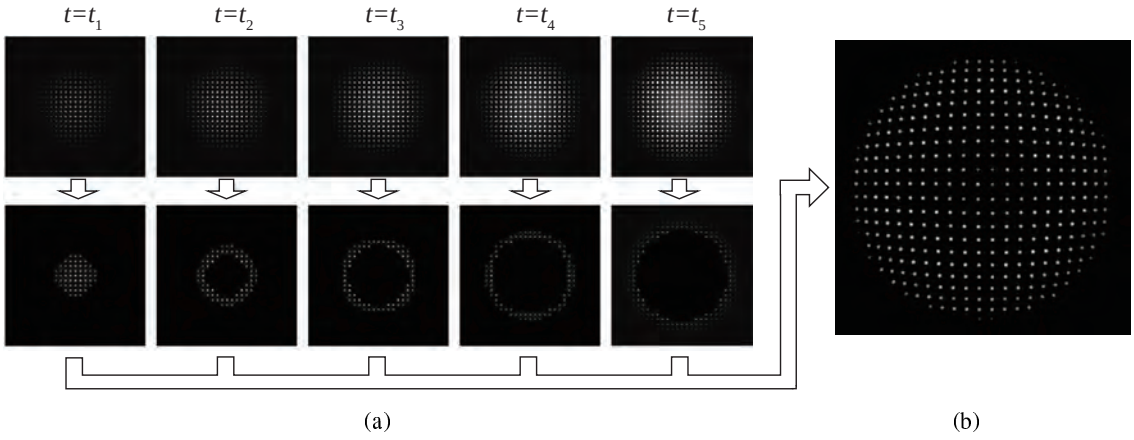

Fig. 4. Hartmanngram combined with different exposure frames.

From Fig. 4, we can see the faint spots at outside of short exposure frame, and also the saturated spots around center of long exposure frame. Therefore, we selected the data from all the exposures as follows. First, in order to select

enough bright spots from the whole Hartmann spots, we choose the longest exposure frame of $t = t_n$, then remove all the saturated spots from it. Next, we also remove the saturated spots from the shorter exposure frame of $t = t_{n-1}$. This procedure is repeated up to the exposure frame of $t = t_1$. Finally, we add the segmented image from each frames under the condition to reject the low signal to noise (SNR) spots. As a results, enough bright spots aligned in the annulus at each frames as shown in the left lower rows of Fig. 4 are accumulated. The resultant Hartmann spots are shown in right portion of Fig. 4. In spite of the above illuminance correction, we can see the illuminance of Hartmann spots is non-uniform. Note that the distribution of SNR rather than illuminance must be uniform over the all Hartmann spots because Hartmanngram is only used for centroiding calculation. Therefore, non-uniform of illuminance distribution such as Fig. 4 can be neglected.

2.2. Pairing algorithm for highly distorted Hartmann spots

As mentioned in section 1, the spot displacement δ_i is proportion to the wavefront slope θ_i, and is also expressed as the distance from the center of lenslet on the detector plane to the centroid of focal spot. However multiple spots or crossed-over spots could appear in the same sub-aperture in Hartmanngram if the incident wavefront is highly aberrated. In this case, we cannot identify the location of the ith focal spots corresponding to the ith sub-aperture lens by which the incident wavefront was segmented [6]. In order to avoid this labeling error, we propose a simple algorithm to determine the relation between the Hartmann spots to the sub-aperture lens. Note that we only modify the pairing algorithm without using a special holographic sub-aperture or a spatial mask for lenslets.

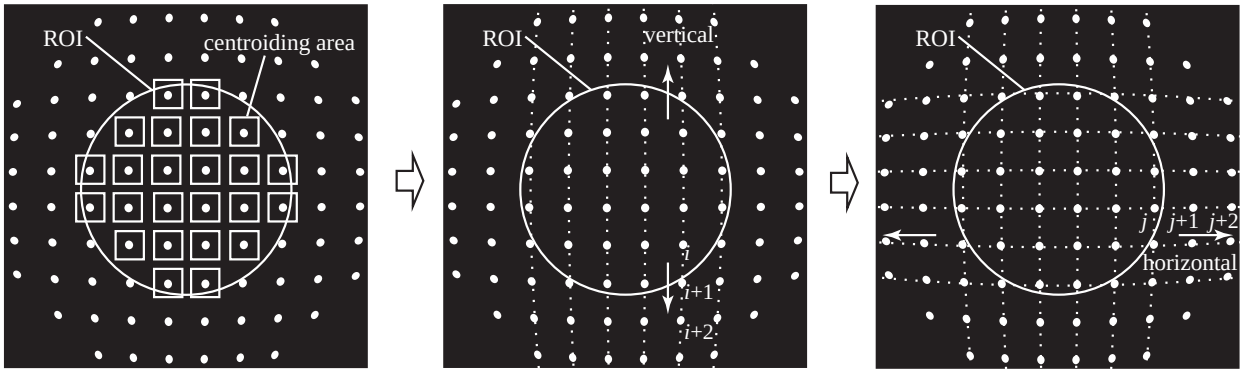

(a) (b) (c)

Fig. 5. A new algorithm to determine the relation between the lenslet and the focal spot.

At first, Fig. 3(b) shows the example of Hartmanngram with the incident distorted wavefront. The displacement of focal spots in Fig. 3(b) is proportionally increasing with the distance from center. Therefore, we set the region of interest (ROI) around the center of image sensor as shown in Fig. 5(a), and calculating the centroid of the spots in the ROI [7]. Next, since the spots are seemed to be aligned as arc-like curves represented by dashed line in Fig. 5(b), the spot of the next lenslet can be estimated from the extrapolation of a series of spots in the ROI. As a result, all the displacement δ_i of the ith sub-aperture can be obtained since we can decide the relationship between the focal spots to the lenslets for all columns and rows.

Fig. 6 shows the related centroiding areas superposed on the highly aberrated Hartmanngram. The measurement result of defocus ~ 11.4 λ and spherical aberration ~ 6.5 λ (λ = 1064 nm) is shown in the Fig. 6(a), and also Fig. 6(b) shows the measurement result of Coma ~ 12 λ. In Fig. 6(a)–(b), white points indicate focal spots and green squares indicate the centroiding area of the related lenslets. In spite of the image distortion, we can see that green squares are aligned on vertcial and horizontal arc-like curves.

Right portion of Fig. 6(a)–(b) show the cross sectional view of obtained wavefront, respectively. Note that the cross

sectional view of Fig. 6(a) is already removed defocus aberration from measured wavefront. Both results show that highly distorted wavefront over 10 λ can be measured by using the proposed paring algorithm.

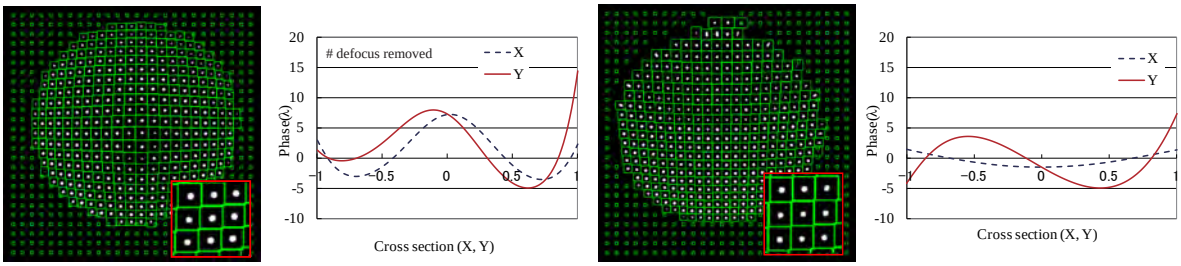

Fig. 6. Example of Hartmanngram with the related centroid areas for highly aberrated wavefront.

Finally, in order to verify linearity and dynamic range of aberrated wavefront, we have designed the lens pair which is capable to generate a coma aberration of 10 λ, and/or spherical aberration of +7.5/−1.5 λ. The linearity of testing SHWFS is shown in Fig. 7. The horizontal axis of Fig. 7 is the designed value of coma aberration generated by

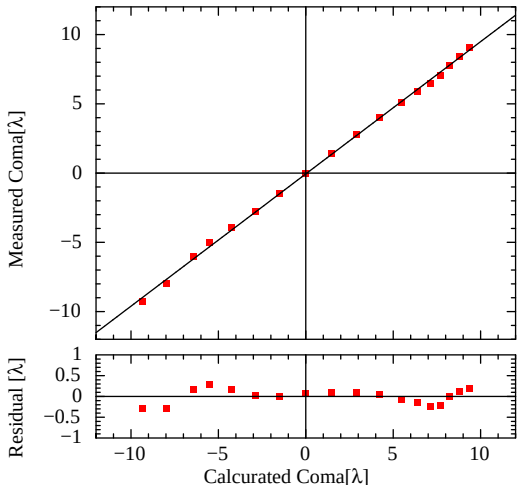

Fig. 7. Measurement results of wavefront errors.

decenter of each lens, and vertical axis is the measurement result obtained from proposed SHWFS. The solid line shows the best-fit value with the linear function with the correlation coefficient of 0.9996. The lower rows of Fig. 7 show residuals from the best-fit model. As the result, it is confirmed that the relation between generated and measured coma aberration is represented by linear function and residual error is less than 0.2 λ in the range of ±10 λ coma aberration.

3. Techniques for speeding up of frame rate

AOI systems provide a means of sensing the atmospheric turbulence-induced aberration and partially correcting for this aberration in real-time. AOI systems must basically perform two main functions: 1) sense the wavefront deformations and 2) compensate in real-time for the deformation. Therefore, AOI systems at least consist of a wavefront sensor to detect the wavefront, and a deformable mirror to correct for the distorted phase.

An adaptive optics system with a closed-loop servo response should reject most of the phase fluctuations. The Greenwood frequency of atmosphere is in the range of tens to hundreds of hertz at the visible spectral range. For example, the closed-loop band width and the frame rate of WFS for an AOI system of Subaru Telescope is 100–200 Hz and 2 kHz, respectively [8].

In this section, we present the prototype SHWFS obtained with the frame rate of 4 kHz [9; 10]. Fig. 8 shows the outside appearance of High-frame rate SHWFS, and design parameters and performance are listed in Tab. 2.

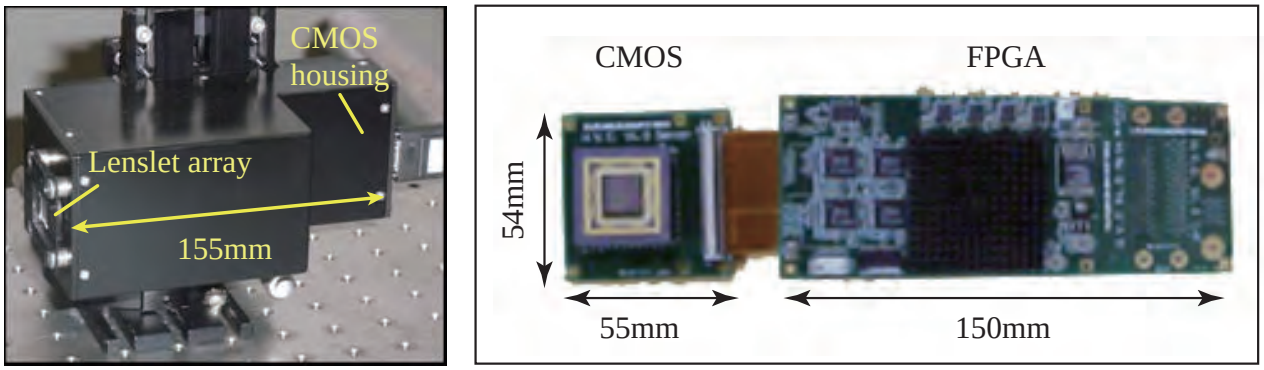

Fig. 8. High-frame rate SHWFS – (a) outside appearance, (b) circuit board.

Tab. 2. Specifications of prototype SHWFS.

Item	Specification	
Number of sub-apertures	10×10	
Upper spatial resolution	4 th order Zernike mode	
Interval of lenslets	0.3mm	
Focal length of lenslets	18mm	
Image sensor type	CMOS image sensor	
	crop readout mode	normal readout mode
Frame rate	4 kHz	2 kHz
Dynamic range	4 λ@633 nm	9 λ@633 nm
Accuracy	$< 1/100\ \lambda$ RMS	$< 1/170\ \lambda$ RMS
Number of readout pixels	$152 \times 7 \times 10$	152×150

3.1. Switchable readout mode

The frame rate of SHWFS is limited by the readout speed of two dimensional imaging device such as CCD or CMOS, and is generally inverse proportional to the number of readout pixels. Therefore, we define two typical ROI region for normal and crop readout mode in order to reduce the number of readout pixels [11]. Fig. 9 shows the schematic drawing of two typical operation mode. Upper rows of Fig. 9 show an example of operation mode named as normal readout. Note that readout sensor size is croped by user defined ROI instead of all pixels on the area sensor. The image sensor of the prototype SHWFS consists of 512×512 pixels with pixel pitch of 20 μm. As shown in Tab. 2, the footprint area of 10×10 sub-aperture lens consists of 152×150 pixels. Since the most of pixels are not used for

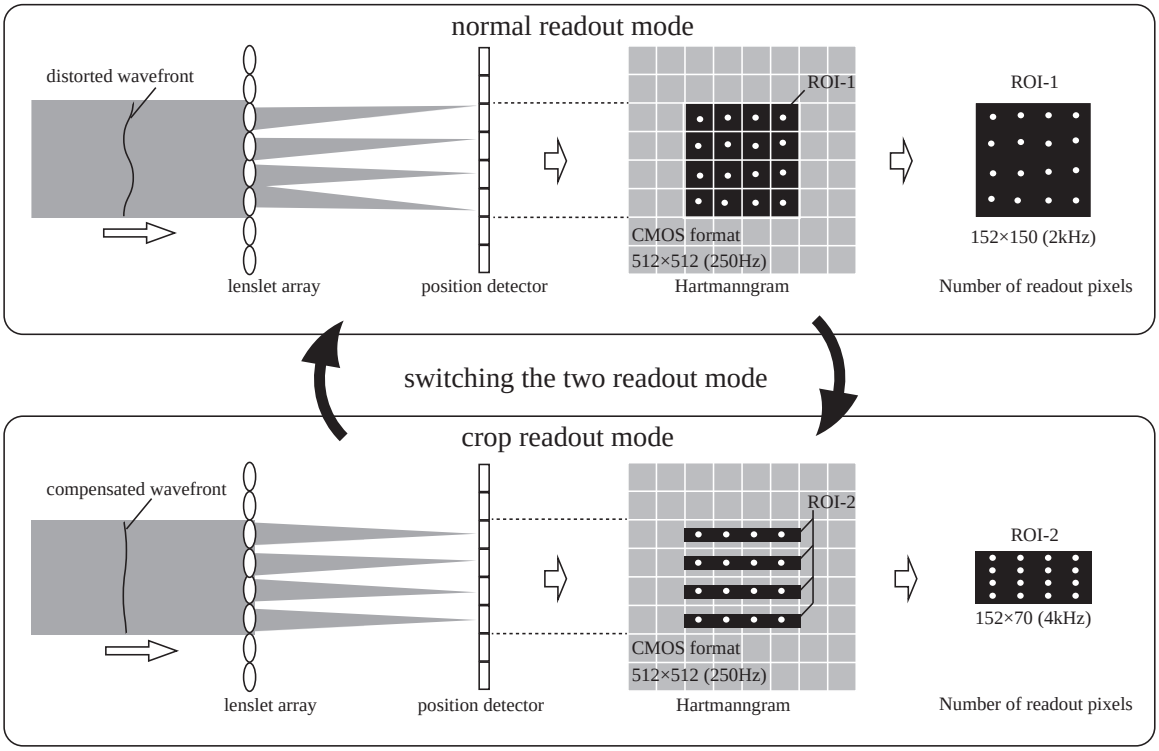

Fig. 9. Two typical operation modes: normal readout mode and crop readout mode.

centroiding calculation, the ROI-1 as shown in Fig. 9 is defined by this footprints area. Since the number of pixels in ROI-1 whose size of 152×150 pixels is quite smaller than that of the image sensor consisting of 512×512 pixels, the elapsed time for readout is effectively reduced. In this case, the frame rate performance is improved from 250 Hz to 2 kHz.

In cases where closed-loop feedback in AOI system is stable, the displacement of focal spots remains so small with the scale of pixel, because wavefront aberrations caused by turbulence in the atmosphere are partially compensated. Therefore, we switch to high speed operation mode named as crop readout. Lower rows of Fig. 9 shows an example of crop readout mode. The readout region of ROI-2 is defined as the sum of narrow horizontal bands around focal spots. In this case of prototype SHWFS, the number of readout pixels is roughly a half of normal readout mode. As a result, the frame rate performance is improved from 2 kHz to 4 kHz.

Finally, the frame rate is successfully speeding up to 2 kHz in normal readout mode, and 4 kHz in crop readout mode because of mode switching and reduction of reading area. Depending on the amount of the compensated wavefront error, it is possible to quickly change the above two operation mode within 10 msec by using FPGA based readout frontend of the CMOS camera.

The wavefront error of each 60,000 frames in the two readout mode is shown in Fig. 10. It shows time series of measured wavefront fluctuation by the SHWFS under stable condition. Fig. 10 also indicates twice faster frame rate of SHWFS in the crop readout mode than the normal readout mode.

The repeatability was 0.0058 λ in 3 σ on normal readout mode, 0.0099 λ on crop readout mode. The error on crop readout mode was quite larger than the other mode because of degrading SNR in proportion to the exposure time. In spite of the fast readout operation, the repeatability of wavefront error still remains in the range of 0.01 λ, and it is enough small to apply for the AOI system.

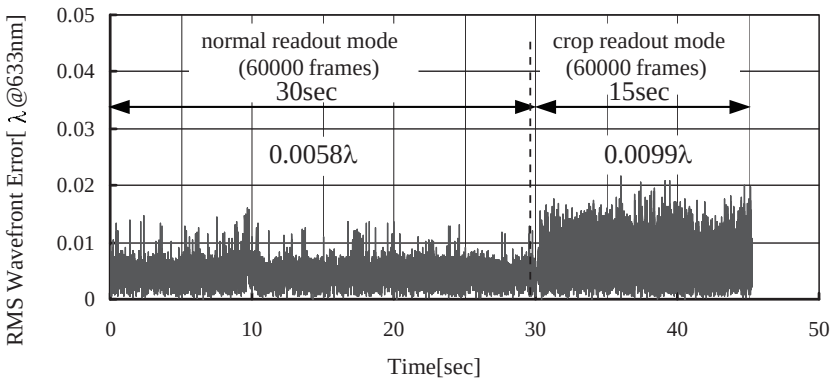

Fig. 10. RMS wavefront error with different operation mode.

4. CONCLUSION

The dynamic-range and frame rate of conventional Shack-Hartmann wavefront sensor are restricted by the size of lenslets and amounts of readout pixels, respectively. In order to improve the measurement performance of conventional SHWFS, we have proposed two main techniques: (1) spots pairing algorithm to increase the dynamic-range of SHWFS, and (2) switching the user defined ROI region to achieve over kHz frame rates. For this purpose, we have introduced these techniques to prototype SHWFS for each, and performed the preliminary experiments to verify performance.

First, after improving the uniformity of Hartmann spots described in section 2.1, we implement a simple algorithm to determine the relation between the lenslets and the focal spots, as is described in section 2.2. As results, we confirmed that a distorted wavefront, such as defocus aberration of 11 μm and spherical aberration of 7μm, can be successfully measured. Furthermore, we also confirmed the linearity of proposed SHWFS with the correlation coefficient of 0.9996 in the range of $\pm$10 μm coma aberration. The residual of wavefront error was less than 0.2 μm in this range.

Next, we have presented high frame rate SHWFS based on crop readout technique with FPGA based CMOS image sensor described in the previous section. We have introduced two typical ROI region for normal and crop readout mode reducing the number of readout pixels. Each readout mode as shown in Fig. 9 can be quickly switched within 10 ms in proportion to slope of incoming wavefront. As a result, frame rate in crop mode is improved twice faster from 2 kHz to 4 kHz, and the repeatability of wavefront error is satisfied < 6 nm RMS. We confirmed that the performance of the proposed prototype SHWFS satisfies the frame rate of 4 kHz and the accuracy of 0.01 λ for 4 th Zernike mode.

5. REFERENCES

1. Tyson, R. *Principles of adaptive optics, Fourth edition*, CRC press, 2015.
2. Suzuki, J., Ando, T., Suzuki, H., Hirano, Y., Wadaka, S., Matsushita, T. and Mikami, I., *Highly Precise Alignment Method for a Space Telescope Using Shack-Hartmann Sensor* (*in Japanese*), KOGAKU, Vol. 35(10), 534–541, 2006.
3. Takato, N., Usuda, T. and Tanaka, W., *Performance of active mirror support of Subaru Telescope*, Large Ground-based Telescopes, Proc. SPIE, Vol. 4837, 2003.
4. Thomas, S., Fusco, T., Tokovinin, A., Nicolle, M., Michau, V. and Rousset, G., *Comparison of centroid computation algorithms in a Shack-Hartmann sensor*, MNRAS, Vol. 371 , 323–336, 2006.
5. Suzuki, J., Ando, T., Endo, T. and Miwa, Y., *Wavefront sensor and Wavefront sensing method*, JP Patent, 6,322,952, 2018.
6. Bedggood, P. and Metha, A.,*Comparison of sorting algorithms to increase the range of Hartmann-Shack aberrometry*, Journal of Biomedical Optics, Vol. 15(6), 067004, 2010.
7. Suzuki, J.,*Wavefront sensor*, JP Patent, 5,289,173, 2013.

8. Watanabe, M., Oya, S., Hayano, Y., Takami, H., Hattori, M., Minowa, Y., Saito, Y., Ito, M., Murakami, N., Iye, M., Guyon, O., Colley, S., Eldred, M., Golota, T. and Dinkins, M., *Implementation of* 188*-element curvature-based wavefront sensor and calibration source unit for the Subaru LGSAO system*, Proc. SPIE, Vol. 7015, 2008.
9. Suzuki, J. and Ando, T., *High-frame rate Shack Hartmann wavefront sensor based on flexible read-out technique for C-MOS image sensor*, Proc. SPIE, Vol. 8395, 2012.
10. Suzuki, J., Ando, T. and Endo, T., *High-frame-rate Wavefront Sensor Based on Flexible Read-Out Technique for C-MOS Image Sensor*, Conference on Lasers and Electro-Optics Pacific Rim (CLEOPR), WF4-7, 2013.
11. Suzuki, J. and Ando, T., *Wavefront sensor and Adaptive optics system*, JP Patent, 5,818,643, 2015.